Diabetologia (2006) 49: 1567–1577
DOI 10.1007/s00125-006-0257-9

ARTICLE

A. Varadi · A. Grant · M. McCormack · T. Nicolson · M. Magistri · K. J. Mitchell · A. P. Halestrap · H. Yuan · B. Schwappach · G. A. Rutter

Intracellular ATP-sensitive K^+ channels in mouse pancreatic beta cells: against a role in organelle cation homeostasis

Received: 12 January 2006 / Accepted: 28 February 2006 / Published online: 12 May 2006

Abstract *Aims/hypothesis:* ATP-sensitive K^+ (K_{ATP}) channels located on the beta cell plasma membrane play a critical role in regulating insulin secretion and are targets for the sulfonylurea class of antihyperglycaemic drugs. Recent reports suggest that these channels may also reside on insulin-containing dense-core vesicles and mitochondria. The aim of this study was to explore these possibilities and to test the hypothesis that vesicle-resident channels play a role in the control of organellar Ca^{2+} concentration or pH. *Methods:* To quantify the subcellular distribution of the pore-forming subunit Kir6.2 and the sulfonylurea binding subunit SUR1 in isolated mouse islets and clonal pancreatic MIN6 beta cells, we used four complementary techniques: immunoelectron microscopy, density gradient fractionation, vesicle immunopurification and fluorescence-activated vesicle isolation. Intravesicular and mitochondrial concentrations of free Ca^{2+} were measured in intact or digitonin-permeabilised MIN6 cells using recombinant, targeted aequorins, and intravesicular pH was measured with the recombinant fluorescent probe pHluorin. *Results:* SUR1 and Kir6.2 immunoreactivity were concentrated on dense-core vesicles and on vesicles plus the endoplasmic reticulum/Golgi network, respectively, in both islets and MIN6 cells. Reactivity to neither subunit was detected on mitochondria. Glibenclamide, tolbutamide and diazoxide all failed to affect Ca^{2+} uptake into mitochondria, and K_{ATP} channel regulators had no significant effect on intravesicular free Ca^{2+} concentrations or vesicular pH. *Conclusions/Interpretation:* A significant proportion of Kir6.2 and SUR1 subunits reside on insulin-secretory vesicles and the distal secretory pathway in mouse beta cells but do not influence intravesicular ion homeostasis. We propose that dense-core vesicles may serve instead as sorting stations for the delivery of channels to the plasma membrane.

Keywords Beta cell · Calcium · Insulin · K_{ATP} · Sulfonylurea · Sulphonylurea

Abbreviations BODIPY-FL: fluorescently labelled boron dipyrromethene difluoride · EGFP: enhanced green fluorescent protein · ER: endoplasmic reticulum · K_{ATP}: ATP-sensitive potassium channel · Kir6.2: inwardly rectifying K^+ channel, 6.2 · LAMP-1: lysosome-associated membrane protein-1 · LDCV: large dense-core insulin-containing vesicle · mGPDH: mitochondrial glycerol phosphate dehydrogenase · SREBP: sterol regulatory element binding protein-1c precursor · SUR1: sulfonylurea receptor-1 · TGN38: *trans*-Golgi network protein 38

Introduction

Elevated glucose concentrations stimulate the secretion of insulin from pancreatic islet beta cells via enhanced metabolism of the sugar and increases in the intracellular ATP:ADP ratio [1, 2]. Closure of ATP-sensitive K^+ (K_{ATP}) channels [3] then causes cell depolarisation, influx of Ca^{2+} and the release of stored insulin [4].

Electronic Supplementary Material Supplementary material is available for this article at http://dx.doi.org/10.1007/s00125-006-0257-9

A. Varadi · A. Grant · T. Nicolson · M. Magistri · K. J. Mitchell · A. P. Halestrap · G. A. Rutter (✉)
Henry Wellcome Laboratories for Integrated Cell Signalling and Department of Biochemistry, School of Medical Sciences, University of Bristol, University Walk, Bristol, BS8 1TD, UK
e-mail: g.a.rutter@bris.ac.uk
Tel.: +44-117-9546401
Fax: +44-117-9288274

A. Varadi · M. McCormack
Genomics Research Institute, Centre for Research in Biomedicine, University of the West of England, Frenchay Campus, Coldharbour Lane, Bristol, BS16 1QY, UK

H. Yuan · B. Schwappach
Centre for Molecular Biology (ZMBH), Heidelberg University, Im Neuenheimer Feld 282, 69120 Heidelberg, Germany

K_{ATP} channels exist as oligomeric structures comprising four copies each of a K^+ channel of the inward rectifier class (Kir6.2), which form the channel pore, and four sulfonylurea receptor-1 (SUR1) subunits [3]. Closure of K_{ATP} channels is pivotal to the actions of both nutrient secretagogues and sulfonylureas; changes in the activity of either subunit leads to defective insulin secretion and glucose homeostasis in rodents [5–7]. Moreover, mutations in either subunit are a common cause of hyperinsulinism in infancy [8, 9], whilst polymorphisms in the *KCNJ11* gene, which generate a form (E23K) of Kir6.2 with decreased activity, are linked to type 2 diabetes in human populations [10–12]. Moreover, mutations in the *KCNJ11* gene are responsible for ~50% of cases of permanent neonatal diabetes mellitus [13–15].

Early work indicated that endogenous Kir6.2 [16] and SUR1 [17] are present on most, if not all, islet cell types in the mouse, but did not resolve the intracellular localisation of the channel. Recent studies [18] have suggested that a significant proportion of the total cellular content of Kir and SUR channels reside on intracellular structures. Studies using fluorescently labelled glibenclamide (a cell-permeant sulfonylurea) and antibody staining [18], demonstrated that K_{ATP} channel complexes are located predominantly on dense-core insulin-containing secretory vesicles, in line with earlier observations [19, 20], and may serve to mediate effects of sulfonylureas [21]. However, Quesada et al. [22] reported binding of fluorescently labelled glibenclamide–boron dipyrromethene difluoride (glibenclamide-BODIPY-FL) principally to the nuclear envelope of primary beta cells.

Smith et al. [23] have proposed that mitochondrial K_{ATP} channels, reportedly present on mitochondria in both liver [24] and heart [25], may mediate some of the effects on sulfonylureas in beta cells. Acting via these channels, diazoxide may also reduce the mitochondrial membrane potential, and therefore ATP synthesis [26]. However, Garlid has pointed out that it is unlikely that sufficient mitochondrial K_{ATP} channel activity is present to mediate such an effect [27].

A potential criticism of previous immunocytochemical investigations [18] has been uncertainty as to the identity of the bound antigen. Here, by combining complementary fractionation, immunopurification and immunocytochemical approaches, we have investigated the subcellular localisation of Kir6.2 and SUR1 in isolated islets and clonal MIN6 beta cells. The latter cells retain many of the properties of the parental mouse beta cells, including efficient synthesis and storage of insulin and glucose-stimulated insulin secretion [28].

We demonstrate the presence of the majority of cellular immunoreactive Kir6.2 and SUR1 on dense vesicles and the distal secretory pathway, and the absence of these channel subunits from mitochondrial membranes. However, arguing against an important role for vesicular K_{ATP} channels in intracellular ion homeostasis, Ca^{2+} uptake into neither organelle was affected by K_{ATP} channel regulators.

Materials and methods

Materials Cell culture reagents were from GibcoBRL (Life Science Research, Paisley, UK) and molecular biologicals from Roche Diagnostics (Lewes, UK). Alexa Fluor goat anti-rabbit or anti-guinea pig 488 and 568 secondary antibodies were from Molecular Probes (Eugene, OR, USA). Guinea pig polyclonal anti-insulin antibody was from DAKO (Glostrup, Denmark). Guinea pig polyclonal anti-Kir6.2 antibody was raised against a peptide comprising the last 36 amino acids of Kir6.2 [29], and rabbit polyclonal anti-SUR antibodies against a peptide epitope comprising amino acids 625–650 of hamster SUR1 (unpurified serum used for western blotting) and against a peptide epitope comprising amino acids 743–760 of rat SUR1 (purified antibody used for immunoelectron microscopy). Rabbit polyclonal anti-glycerol phosphate dehydrogenase (mGPDH; mitochondrial marker) antibody was from Sigma (Poole, UK), and rabbit polyclonal anti-phogrin antibody (against amino acids 629–1003) was a kind gift from J. Hutton (Barbara Davis Center for Childhood Diabetes, Denver, CO, USA) [30]. Rabbit polyclonal anti-*trans*-Golgi network protein 38 (TGN38) [31] and mouse monoclonal anti-human lysosome-associated membrane protein-1 (LAMP-1) specific antibodies were kindly provided by G. Banting (University of Bristol, Bristol, UK). Rabbit polyclonal anti-insulin receptor antibody was from Santa Cruz Biotechnology (Mile Elm, UK). Mouse monoclonal anti-sterol regulatory element binding protein-1c precursor (SREBP) [32] was from F. Foufelle (Unit 465 INSERM, Paris, France). Rabbit polyclonal anti-14-3-3-β antibody was raised against a peptide mapping at the amino terminus of the human protein (Autogen Bioclear UK, Mile Elm, UK). OptiPrep, a solution of iodixanol, was from Axis-Shield (Oslo, Norway).

Islet isolation and cell culture Mouse islets were freshly isolated as described previously [33]. MIN6 pancreatic beta cells (at passages 19–35) were cultured in DMEM supplemented with 15% (v/v) foetal calf serum (FCS), penicillin (100 U/ml), streptomycin (0.1 mg/ml), β-mercaptoethanol and L-glutamine (2 mmol/l) at 37°C in an atmosphere of humidified air (95%) and CO_2 (5%) [34].

Subcellular fractionation using OptiPrep iso-osmotic density gradient centrifugation Cells were homogenised in 0.3 mol/l sucrose, 1 mmol/l EDTA, 1 mmol/l $MgSO_4$, 10 mmol/l 2-(*N*-morpholino)ethanesulfonic acid (MES)-NaOH (pH 6.5); 1 μmol/l phenylmethylsulfonyl fluoride (PMSF), 5 μg/ml aprotinin, and 5 μg/ml leupeptin using a ball-bearing homogeniser, and then centrifuged at 500 *g* for 10 min. The post-nuclear supernatant was layered on top of a continuous 8–19% (w/v) OptiPrep gradient obtained using a Gradient Master (BioComp Instruments, Fredericton, NB, Canada) and centrifuged at 16, 000 *g* for 16 h. Gradient fractions were collected by downward displacement (Gradient station; BioComp Instruments).

Detection of Kir6.2 and SUR in subcellular fractions of MIN6 cells Equal volumes from the gradient fractions were separated on 9% (w/v) polyacrylamide gels then blotted onto Immobilon-P transfer membrane (Millipore, Watford, UK) and probed with organelle-specific antibodies against mGPDH (mitochondria), phogrin (large dense-core insulin-containing vesicle [LDCV] membranes) [30, 35], TGN38 (Golgi) [31], insulin receptor (IR, plasma membrane); LAMP-1 (lysosomes) [36]; SREBP precursor (endoplasmic reticulum [ER]) [32]; 14-3-3-β (cytosol) [37]. The protein and insulin contents in each fraction were determined using a Pierce BCA Protein Assay Kit (Rockford, IL, USA) and a Mercodia Ultrasensitive Mouse Insulin ELISA Kit (Uppsala, Sweden), respectively.

FACS sorting of phogrin.EGFP-containing vesicles and precipitation with trichloroacetic acid MIN6 cells were infected with the recombinant phogrin.enhanced green fluorescent protein (EGFP) adenoviral construct, at a multiplicity of 30–100 viral particles/cell, for 1 h. Cells were subsequently used 24 h post infection when >95% of cells were infected. Cells were scraped into ice-cold buffer containing 10 mmol/l 3-(*N*-morpholino)propanesulfonic acid (MOPS), 260 mmol/l sucrose (pH 6.5), 1 mmol/l PMSF, 5 μg/ml aprotinin and 5 μg/ml leupeptin, then homogenised with a Teflon homogeniser and centrifuged at 500 *g* for 5 min. The post-nuclear supernatant was resuspended in MOPS buffer to a concentration of 1–2 mg/ml and sorted into two fractions: (1) particles labelled with EGFP, and (2) unlabelled organelles. Sorting was carried out on a FACS Vantage sorter (Becton Dickinson, Oxford, UK) fitted with a 488-nm argon ion laser. The EGFP fluorescence was measured using a bandpass filter at 530/30 nm. Following sorting, 7×10^6 vesicles were obtained, and 7×10^4 vesicles were seeded onto poly-L-lysine-coated coverslips and used for immunocytochemistry. The remaining vesicle suspension was treated with an equal volume of 20% (v/v) trichloroacetic acid for 30 min at 4°C, then centrifuged at 13, 000 *g* for 10 min before SDS gel electrophoresis.

Immunocytochemistry FACS-sorted vesicles on glass coverslips were fixed for 10 min in 4% (w/v) paraformaldehyde in PBS at room temperature, followed by washing in PBS (5 min). Vesicles were incubated in 100 mmol/l glycine in PBS (pH 8.5) for 5 min and then 10% (v/v) FCS in PBS (5 min), before permeabilisation in 0.2% (v/v) Triton X-100 in PBS (20 min) at room temperature. This was followed by blocking in 3% (w/v) BSA in PBS for 15 min. Cells were then incubated with the primary antibodies overnight and with the secondary antibodies for 1.5 h at room temperature in 3% (w/v) BSA in PBS, before mounting and confocal imaging as described previously [38].

Images were captured on a Nipkov disc-based UltraVIEW confocal system (PerkinElmer Life Sciences, Boston, MA,USA) [39] using a 63× PL Apo 1.4NA oil-immersion objective lens (Leica, Heidelberg, Germany).

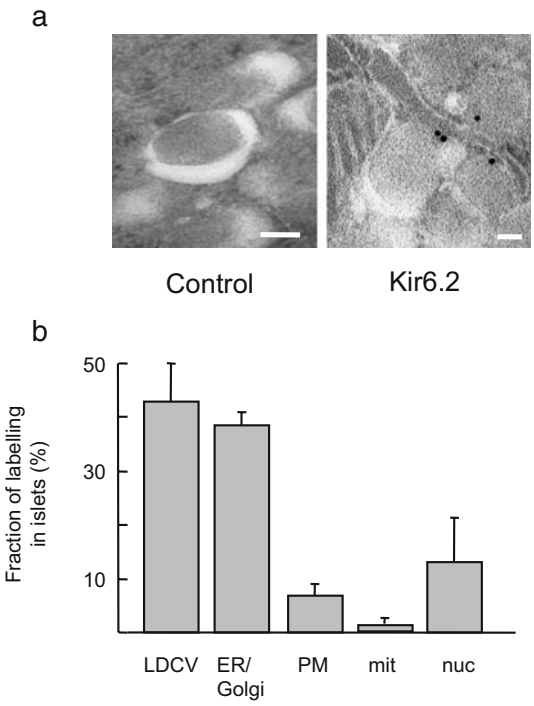

Fig. 1 Kir6.2 localises to dense-core vesicles and ER/Golgi of primary mouse islets examined by immunoelectron microscopy. **a** Islets were fixed and embedded as described (see Materials and methods) and then incubated with either no primary antibody (control) or anti-Kir6.2 antibody (1:10 dilution) before being visualised with a goat anti-guinea pig (10 nm) gold-conjugated secondary antibody (1:20). The mean number of particles per 8.1 μm^2 area at ×31,000 magnification was 58±10 (*n*=8 areas). Similar data (not shown) were obtained after co-staining for insulin. Note the localisation of immunoreactivity at the periphery of dense-core vesicles. Scale bars=100 nm. **b** Distribution of gold particle labelling on morphologically identified subcellular structures. *Mit* Mitochondria, *nuc* nucleus, *PM* plasma membrane, *ER* endoplasmic reticulum, *LDCV* large dense core vesicles

Immunoabsorption of phogrin EGFP-containing vesicles. Phogrin.EGFP-infected cells were homogenised as described previously [40]. The post-nuclear supernatant was further centrifuged at 2,400 *g* for 10 min at 4°C, and the pellet was resuspended in buffer B (50 mmol/l HEPES, 1 mmol/l EDTA, 150 mmol/l NaCl, 1 μmol/l PMSF, 5 μg/ml aprotinin and 5 μg/ml leupeptin) to a concentration of 1–2 mg/ml. A sample (100–200 μg) of homogenate was pre-cleared with 100 μl of packed Protein-A sepharose in buffer B overnight, and then centrifuged at 14,000 ×*g* for 3 s. Anti-EGFP antibody (20 μl) was first incubated with 50 μl Protein-A sepharose in buffer B. Pre-cleared samples (150–250 μl) were added to the antibody-bound beads, and incubation continued for a further 24 h at 4°C. Samples were centrifuged at 500 *g* for 30 s, and the immunoadsorbed vesicles were washed four times with buffer B and analysed by SDS-PAGE and immunoblotting [41]. Immunostaining was revealed with horseradish peroxidase-conjugated anti-guinea pig IgG (1:5,000 dilution) and anti-rabbit IgG (1:40,000 dilution) using an enhanced chemiluminescence (ECL) detection system.

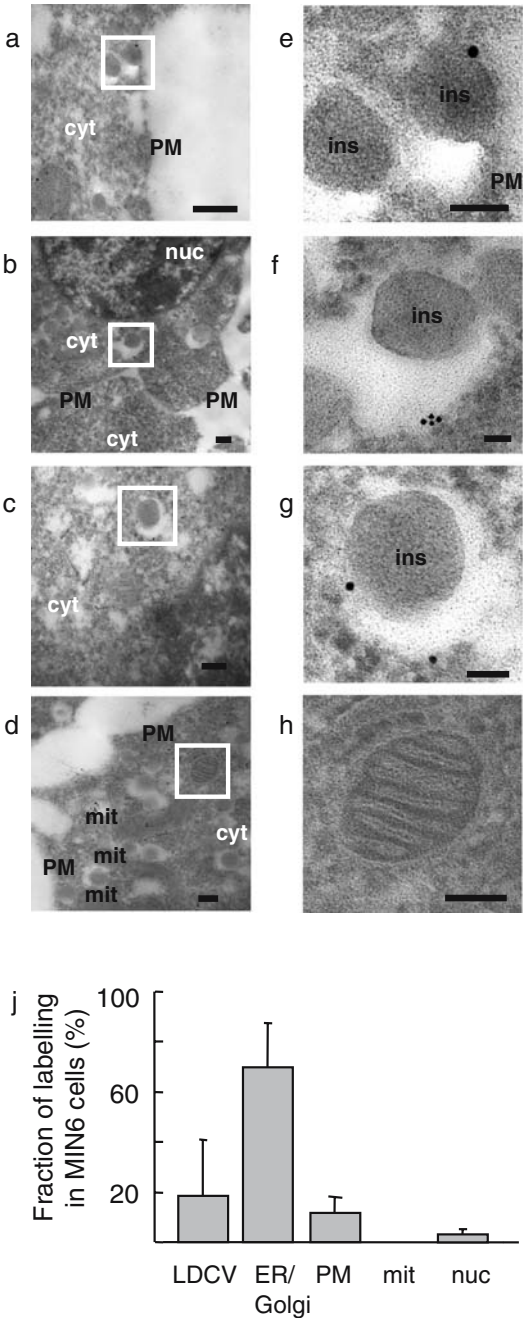

Fig. 2 Kir6.2 localises to dense-core vesicles and ER/Golgi of MIN6 cells examined by immunoelectron microscopy. Cells were fixed and embedded as in Fig. 1. *Boxed areas* in **a–d** are shown on an expanded scale in **e–h**. Image **h** shows a single mitochondrion. Scale bars=100 nm (**a–d**) or 50 nm (**e–h**). Panel **j** shows the distribution of gold particle labelling on morphologically identified intracellular structures. *Cyt* Cytosol, *ins* insulin, *mit* mitochondria, *nuc* nucleus, *PM* plasma membrane

Postembedding immunocytochemistry and electron microscopy Islets or MIN6 cell pellets were fixed in 4% paraformaldehyde and 0.1% glutaraldehyde in 0.1 mol/l sodium cacodylate buffer (pH 7.4) containing 3 μmol/l $CaCl_2$ at 37°C, and allowed to cool to room temperature for 4 h. LR White resin-embedded ultrathin (70–150 nm) sections were picked up on uncoated nickel slot grids and

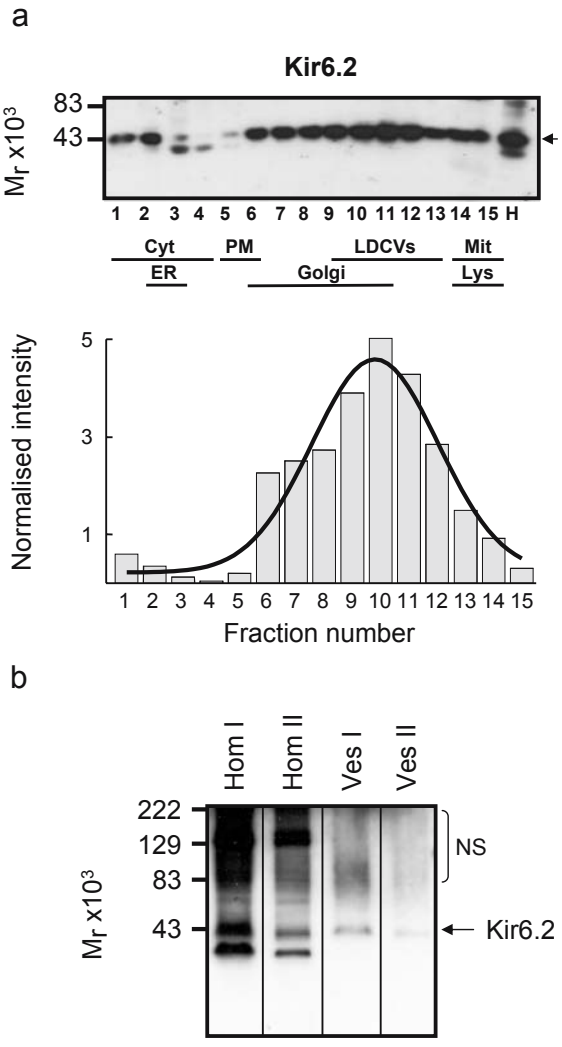

Fig. 3 Kir6.2 is associated with insulin-containing vesicles and Golgi fractions by MIN6 cell fractionation. **a** Density gradient analysis. MIN6 cell homogenates were fractionated by OptiPrep density gradient centrifugation and the subcellular fractions were separated by SDS gel electrophoresis and the immunoblots probed with a guinea pig polyclonal anti-Kir6.2 antibody. The blot was scanned and quantified with NIH ImageJ software http://rsb.info.nih.gov/ij/, last accessed in March 2006). The intensity of bands was normalised to protein content. The continuous lines represent the Gaussian distribution of Kir6.2. See Materials and methods section and ESM figures for details of organelle marker distribution. *Cyt* Cytosol, *H* homogenate, *Lys* lysosomes, *Mit* mitochondria, *PM* plasma membrane. **b** Vesicle immuno-isolation. Cells were infected with the recombinant phogrin.EGFP adenoviral construct and homogenised 24 h after infection (Hom I and II). Phogrin.EGFP-containing vesicles were then immunoadsorbed using a monoclonal anti-EGFP antibody (Ves I and II). The immunoadsorbed vesicles were analysed by 15% SDS-PAGE and immunoblotting. The blot was probed with a guinea pig polyclonal anti-Kir6.2 antibody. The *arrow* shows the position of Kir6.2. Samples containing 20 and 10 μg protein were loaded on lanes Hom I and Hom II, respectively. Samples containing 200 and 100 μg of cell homogenate were used as starting material for immunoadsorption on lanes Ves I and Ves II, respectively. *NS* Non-specific immunostaining, *ESM* electronscanning microscope

were incubated on blocking solution, which consisted of 50 mmol/l Tris (pH 7.4) containing 0.9% NaCl (TBS),

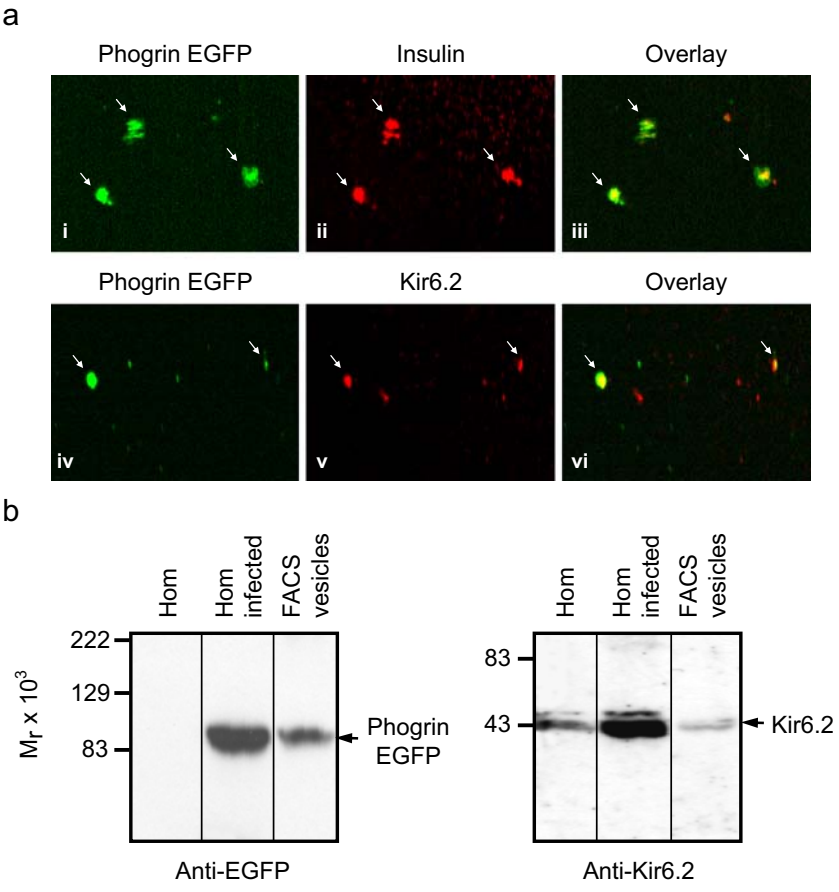

Fig. 4 Kir6.2 is present on single FACS-sorted phogrin. EGFP vesicles. MIN6 cells were infected with the recombinant phogrin.EGFP adenoviral construct, and fluorescent EGFP-labelled vesicles were separated from non-labelled organelles by FACS sorting. **a** FACS-sorted vesicles were seeded onto poly-L-lysine-coated coverslips and immunostained with a guinea pig polyclonal anti-insulin antibody or a guinea pig polyclonal anti-Kir6.2 antibody, then visualised with an Alexa Fluor goat anti-guinea pig 568 secondary antibody (**ii, v**). Phogrin.EGFP fluorescence is shown in **i** and **iv**. Overlays of **i** and **ii**, **iv** and **v** are shown in **iii** and **vi**, respectively. **b** The sorted vesicle proteins (8×10^6 fluorescent particles) were precipitated with trichloric acid then separated on an SDS gel and the immunoblot probed with the guinea pig polyclonal anti-Kir6.2 or the mouse monoclonal anti-EGFP antibody. *FACS vesicles*, FACS-sorted phogrin.EGFP vesicles; *Hom*, homogenate prepared from uninfected MIN6 cells; *Hom infected*, homogenate prepared from MIN6 cells expressing phogrin. EGFP

0.1% Tween-20 and 2% BSA for 1 h. Sections were then incubated overnight at 4°C with immunopurified primary antibodies against insulin (25 μg/ml), Kir6.2 (5–50 μg/ml) and SUR1 (15–30 μg/ml). Sections were then incubated with goat anti-rabbit or goat anti-guinea pig IgG coupled to gold particles (10 nm diameter; 1:100; Nanopores, Stony Brook, NY, USA or BioCell International) for 2 h at room temperature. Selective labelling was not detected in the absence of primary antibodies. Cells were randomly chosen and photographed at 31,000× magnification using a Philips/FEI CM10 transmission electron microscope (Cambridge, UK).

Measurement of mitochondrial and vesicular-free Ca^{2+} concentration and pH MIN6 cells were seeded onto glass coverslips coated with 13 mmol/l poly-L-lysine, and then grown to 50–80% confluence. Cells were infected [42] with adenoviruses encoding untargeted aequorin (AdCMVcytoAq) [43], aequorin targeted to the mitochondria (AdCMVmAq) [42], or mutant aequorin targeted to secretory vesicles (AdCMVVampAq) [44].

Aequorin was reconstituted with 5 μmol/l coelenterazine (LUX Biotechnology, Edinburgh, UK) by incubating for 2 h at 37°C in modified Krebs–Ringer bicarbonate buffer (KRB) (140 mmol/l NaCl, 3.5 mmol/l KCl, 0.5 mmol/l NaH_2PO_4, 0.5 mmol/l $MgSO_4$, 3 mmol/l glucose, 10 mmol/l HEPES, 2 mmol/l $NaHCO_3$, pH 7.4) supplemented with 1.5 mmol/l $CaCl_2$. For reconstitution of VAMPAq, cells were depleted of Ca^{2+} by incubation with the Ca^{2+} ionophore ionomycin (10 μmol/l), the Na^+/H^+ exchanger monensin (10 μmol/l), and the SERCA inhibitor cyclopiazonic acid (10 μmol/l) in Ca^{2+}-free KRB supplemented with 1 mmol/l EGTA, for 5 min at 4°C [45] prior to the addition of 5 μmol/l coelenterazine and further incubation for 2 h at 4°C in KRB supplemented with 100 μmol/l EGTA.

Intact cells were perifused at 37°C in a thermostatic chamber close to a photomultiplier tube (Thales UK, Addlestone, UK) [46]. For experiments on permeabilised cells, an intracellular buffer (IB) was used (140 mmol/l KCl, 10 mmol/l NaCl, 1 mmol/l KH_2PO_4, 1 mmol/l ATP, 5.5 mmol/l glucose, 20 mmol/l HEPES and varying concentrations of $MgSO_4$ and $CaCl_2$, pH 7.05, plus 2 mmol/l Na^+ succinate, unless otherwise stated. IB was buffered with 0.2 mmol/l EGTA and 1 mmol/l HEDTA, and the free [Ca^{2+}] and [Mg^{2+}] (usually 0.5 mmol/l) were calculated using 'METLIG' [47]. MIN6 cells were initially perifused with KRB supplemented with 100 μmol/l EGTA before permeabilising with 20 μmol/l digitonin in IB for 1 min at 37°C. Aequorin calibration was as described previously [44, 48]. Vesicular pH was measured using ecliptic pHluorin and confocal microscopy [44].

Statistical analysis Data are presented as the means±SEM for 3–6 separate experiments, and statistical significance calculated using the Student's *t*-test.

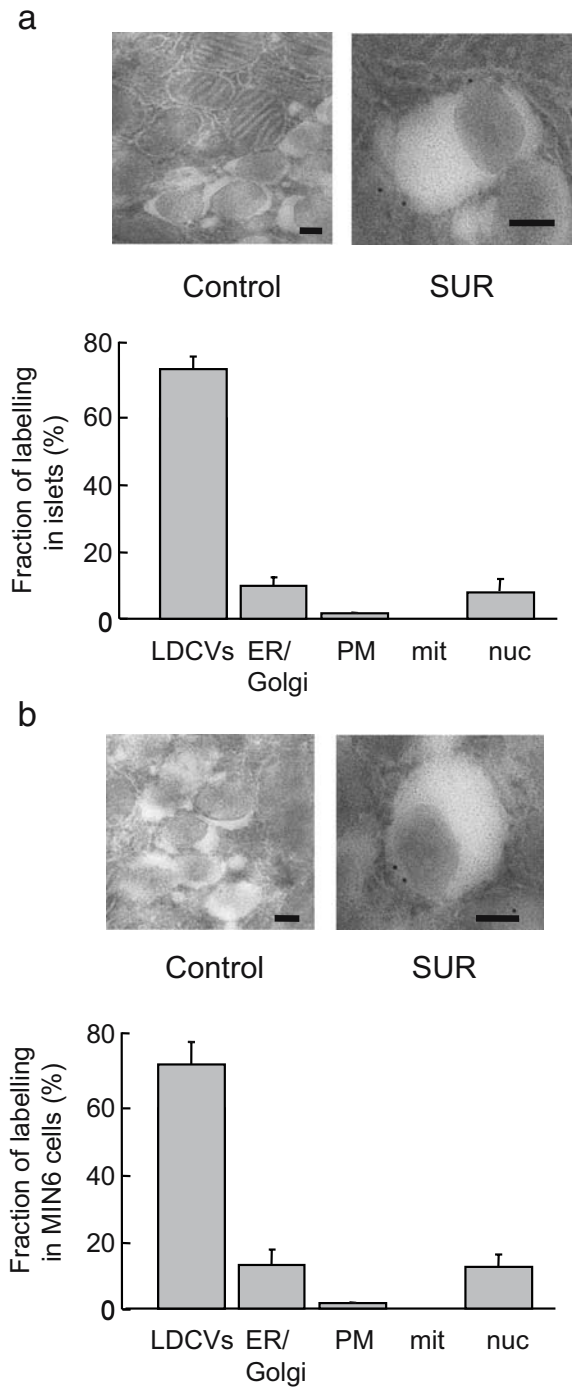

Fig. 5 Immunolocalisation of SUR1 by electron microscopy. Mouse islets (**a**) or MIN6 cells (**b**) were fixed and embedded as described (Fig. 1), and gold particle distribution quantified after treatment with anti-SUR1 antibodies (SUR), or in the absence of primary antibody (control). Note that the graphs demonstrate clearly the presence of immunoreactivity associated with dense-core vesicles in each case, and the absence of reactivity on mitochondria. *Mit* Mitochondria, *nuc* nucleus, *PM* plasma membrane. Scale bar=100 nm

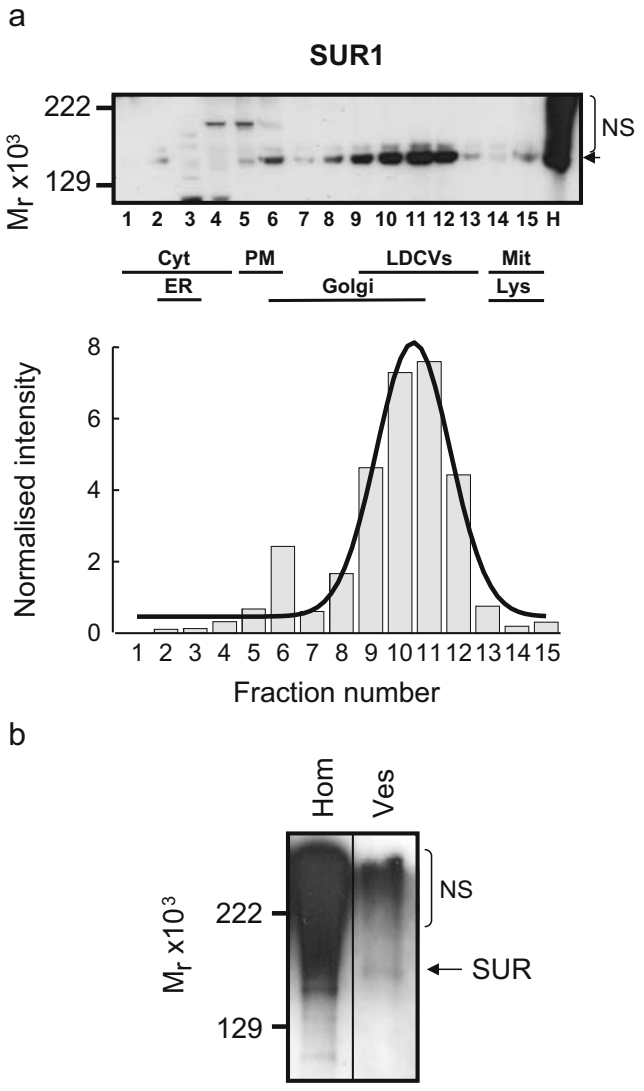

Fig. 6 SUR1 is associated with insulin-containing vesicles and the Golgi. **a** MIN6 cell homogenates were fractionated by OptiPrep density gradient centrifugation. The subcellular fractions were separated by SDS gel electrophoresis and the immunoblots probed with a rabbit polyclonal anti-SUR antibody (for details see Fig. 3). **b** Cells were infected with the recombinant phogrin.EGFP adenoviral construct and homogenised 24 h after infection (*Hom*). Phogrin.EGFP-containing vesicles were then immunoadsorbed (*Ves*) and analysed by 15% SDS-PAGE and immunoblotting (see Fig. 3). The blot was probed with a rabbit polyclonal anti-SUR antibody. Molecular weight markers are indicated on the left, and the arrow shows the position of SUR. *Cyt* Cytosol, *Lys* lysosomes, *Mit* mitochondria, *NS* non-specific immunostaining

Results

Subcellular localisation of Kir6.2 Examined in primary mouse islets, electron microscopy analysis revealed the presence of Kir6.2 reactivity on the limiting membrane of LDCVs, on internal membranes likely to correspond to the ER/Golgi, and on the plasmalemma and nuclear membrane (Fig. 1). A similar distribution, albeit with a greater preponderance of staining on ER/Golgi membranes, was apparent in MIN6 beta cells (Fig. 2). By contrast, no reactivity was detected on mitochondrial membranes in either case (Figs. 1 and 2d,h).

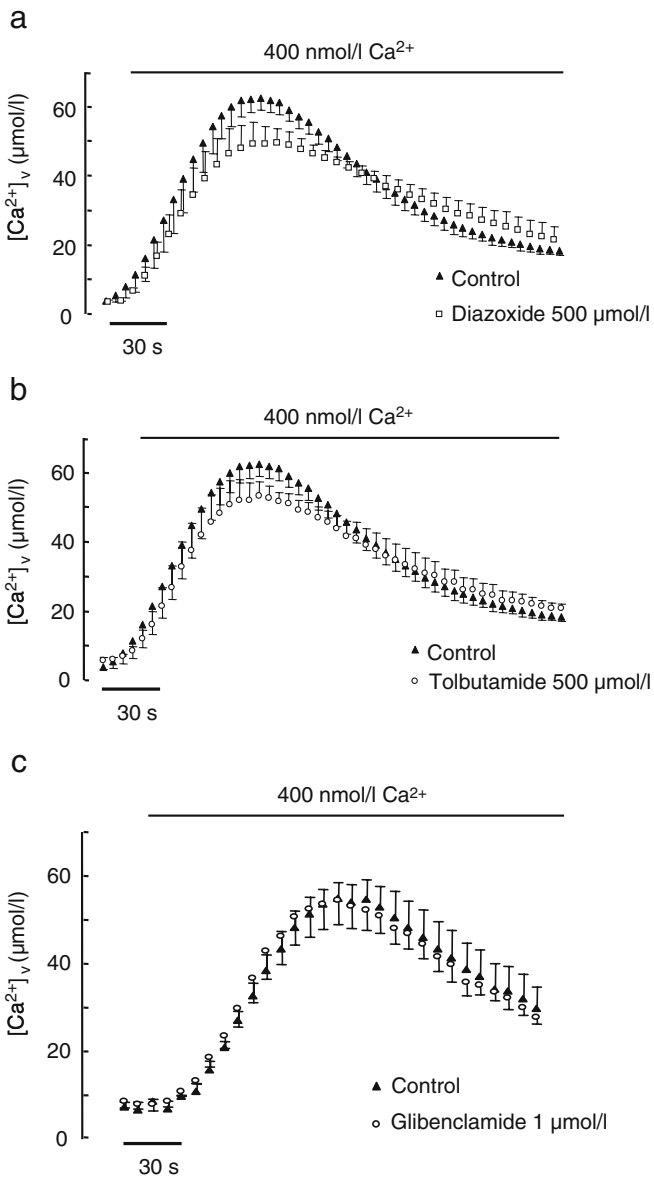

Fig. 7 Effects of K_{ATP} channel inhibitors on vesicular Ca^{2+} accumulation in permeabilised MIN6 cells. Vesicle-targeted aequorin was reconstituted as described (see Materials and methods section) and free intravesicular Ca^{2+} $[Ca^{2+}]_v$ monitored in the initial presence of <1 nmol/l buffered Ca^{2+} and then 400 nmol/l Ca^{2+}, as indicated, in the additional presence of diazoxide (**a**), tolbutamide (**b**) and glibenclamide (**c**). The *closed triangles* in each graph represent the control. Data are the means±SEM of 3 (**a, c**) or 4 (**b**) separate experiments, each involving three replicate runs

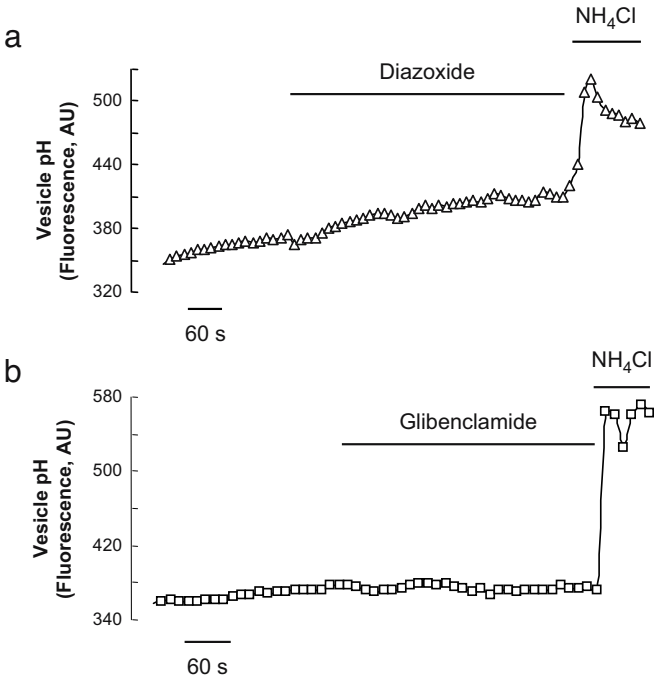

Fig. 8 Effect of K_{ATP} channel regulation on secretory vesicle pH in permeabilised MIN6 beta cells. Cells were perifused in the presence of 100 nmol/l free $[Ca^{2+}]$, and eclipitc pHluorin fluorescence was excited at 488 nm. Emitted light collected at 535 nm. Diazoxide (**a**) or glibenclamide (**b**) were added at 500 and 1 μmol/l, respectively, and NH_4Cl at 10 mmol/l. Data are the means of data from 3 or 4 cells in each case

To confirm the identity of the recognised epitope, we next used density gradients of iodixanol (OptiPrep) [40] to obtain subcellular factions of MIN6 cells. As shown in Electronic Supplementary Material (ESM) Fig. 1, this technique allowed separation of progressively heavier fractions from those rich in cytosol markers (14-3-3-β protein; fractions 1–5), early endosomes (LAMP-1; fractions 1, 2), ER (SREBP-1 precursor; fractions 2, 3), plasma membrane (insulin receptor; fractions 5 and 6) and Golgi apparatus (TGN38; fractions 8–11). LDCV markers, including phogrin (endogenous and overexpressed) and insulin, were principally found towards the bottom of the gradient, in fractions 9–13 (ESM Fig. 2), but were clear of mitochondrial contaminants (mGPDH, fraction 14).

As shown in Fig. 3, immunoreactivity for Kir6.2 (43 kDa) antibody was detected principally (>90% of total immunoreactivity) on insulin- and Golgi marker-containing fractions (8–12), with an overall distribution similar to that of endogenous phogrin (calculated peak at fraction 9.6±0.16). Kir6.2 positivity was also detected in ER and plasma membrane fractions (2 and 6, respectively) but at low levels, likely to have resulted from contamination with vesicles, in a mitochondrial marker-enriched fraction (14). By contrast, Kir6.2 reactivity was clearly present in immunopurified phogrin. EGFP-positive dense-core vesicles (Fig. 3b) and insulin- or phogrin-containing vesicles isolated by FACS sorting [40] by either immunocytochemistry (Fig. 4a) or immunoblot analysis (Fig. 4b).

Subcellular localisation of SUR1 Immunogold labelling identified LDCVs as the major location of SUR1 immunoreactivity in both islets and MIN6 cells, with more minor labelling of Golgi/ER, plasmalemma and nuclear membranes, but undetectable staining of mitochondria (Fig. 5). Correspondingly, MIN6 cell fractionation (Fig. 6a) revealed SUR1 immunoreactivity (140–150 kDa) concentrated on LDCV-marker-enriched fractions (9–12) and on plasma membrane marker-containing fractions (5, 6), with a calculated mean peak at a higher density (fraction 10.4±0.11) than that for Kir6.2. SUR1 reactivity was barely detected on ER- (2, 3) or

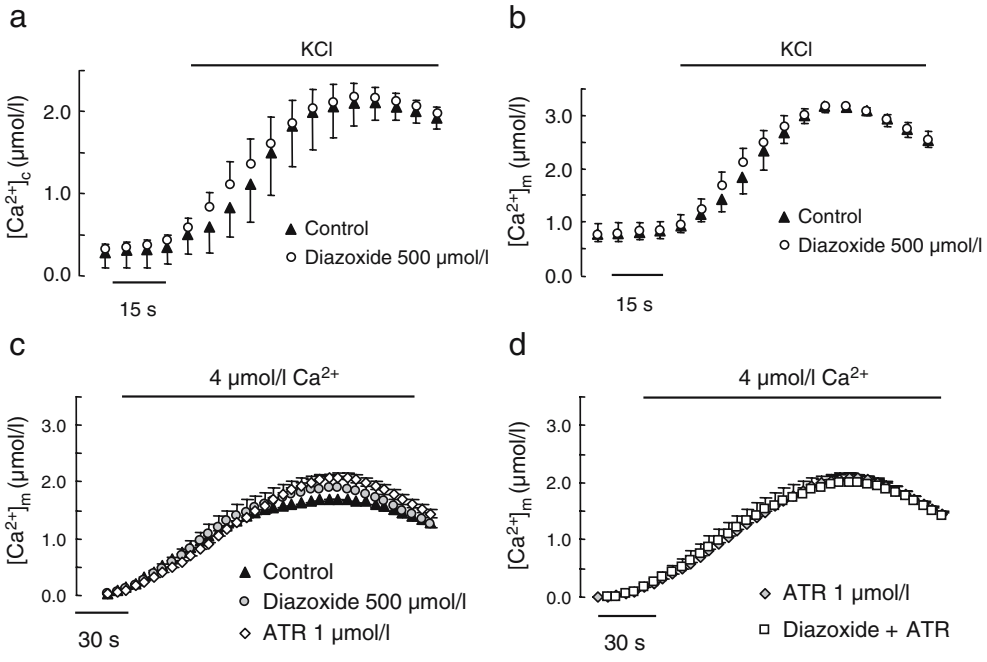

Fig. 9 Effects of diazoxide on mitochondrial Ca^{2+} accumulation. Cytosolic (**a**) and intra mitochondrial (**b**) free Ca^{2+} concentrations were monitored in intact MIN6 cells using suitably targeted aequorins and stimulated with 50 mmol/l KCl (see Materials and methods section). (**c, d**) Ca^{2+} accumulation into mitochondria was assessed in permeabilised MIN6 cells in the absence or presence of diazoxide or atractyloside (ATR), as shown. Perifusion was initially at <1 nmol/l buffered free Ca^{2+}. Data (means±SEM) are from 3 or 4 experiments in each case, each involving three replicates

early endosome-containing fractions (1,2). By contrast, the mitochondria-rich fraction (14) was negative for reactivity (Fig. 6b). SUR1 reactivity was also identified on immunopurified dense-core vesicles (Fig. 6b).

Impact of K_{ATP} channel modulation on intravesicular-free Ca^{2+} and pH To explore the potential role of K_{ATP} channels in vesicular ion homeostasis, intravesicular-free [Ca^{2+}] was measured using an adenovirally expressed VAMP2.aequorin chimera [44]. To eliminate confounding effects of plasma membrane-located K_{ATP} channels, cells were permeabilised with digitonin. Perifusion initially in the absence (<1 nmol/l) of Ca^{2+} and then with a low (near-physiological) [Ca^{2+}] (400 nmol/l) increased intravesicular free [Ca^{2+}] to ~60 μmol/l, as previously reported [44]. Both the K_{ATP} channel opener (diazoxide) and blocker (tolbutamide) exhibited a non-significant tendency to lower the rate and extent of vesicle [Ca^{2+}] increase (Fig. 7a,b; minimum p=0.066 and 0.064 for the effects of diazoxide or tolbutamide, respectively), suggestive of non-specific effects possibly including a protonophore action [23] at the concentrations used. Correspondingly, the more specific channel closer, glibenclamide, did not affect vesicle [Ca^{2+}] increases (Fig. 7c). Similarly, neither diazoxide nor glibenclamide significantly affected intravesicular pH, measured with ecliptic pHluorin (Fig. 8).

Impact of K_{ATP} channel modulation on mitochondrial membrane potential and Ca^{2+} accumulation We next sought to determine whether K_{ATP} channels, although undetectable by biochemical approaches (see above), may nonetheless have a functional role on mitochondria. Recombinant aequorins targeted to the mitochondrial matrix or cytosol [43, 48, 49] were used. As previously demonstrated [42, 48], depolarisation of intact cells with 30 mmol/l KCl caused increases in [Ca^{2+}] in both compartments, with a ~50% greater increase in the mitochondrial matrix, as expected (Fig. 9a,b). These changes were essentially unaffected by the diazoxide (500 μmol/l). Similarly, assayed in permeabilised cells in the presence of glutamate plus malate as respiratory substrates (note that mitochondrial succinate oxidation is inhibited by diazoxide) [50] and at Ca^{2+} concentrations between 1 and 4 μmol/l, diazoxide (500 μmol/l) exerted no effect on the rate or extent of mitochondrial [Ca^{2+}] increase (not shown). Furthermore, similar rates of mitochondrial [Ca^{2+}] change were observed in the presence of atractyloside, an adenine nucleotide translocase (ANT) inhibitor [51], added to increase mitochondrial-free [ATP] [52] (Fig. 9c,d). Thus, increased mitochondrial Ca^{2+} buffering exerted little effect on mitochondrial uptake of the ion under these conditions. Likewise, neither tolbutamide (in the presence of either ADP or ATP) nor glibenclamide exerted any effect on mitochondrial-free [Ca^{2+}] in permeabilised cells (Fig. 10).

Discussion

Using complementary immunoelectron microscopy, cell fractionation and vesicle purification approaches, we show here that the subunits of the beta cell K_{ATP} channel are present chiefly on dense-core secretory vesicles but also more proximal regions of the secretory pathway in primary and clonal mouse beta cells. These data therefore refine a recent report [18] suggesting localisation of both subunits to LDCVs alone. In contrast, we failed to detect any immunoreactivity against either of the two classical beta cell K_{ATP} channel subunits on mitochondrial membranes (Figs. 1, 2, 3, 4, 5 and 6) or any pharmacological evidence

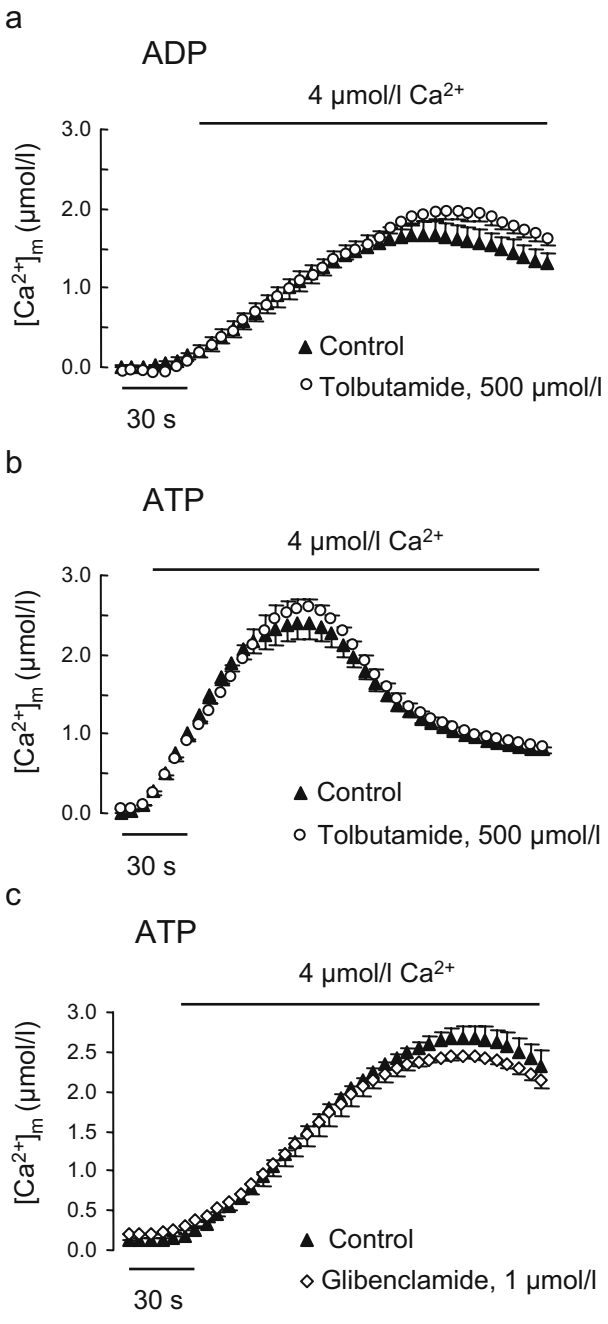

Fig. 10 Effects of K_{ATP} channel inhibitors on mitochondrial Ca^{2+} accumulation in permeabilised MIN6 cells. Mitochondrial free Ca^{2+} concentration was monitored as described (see Materials and methods section and legend to Fig. 7) in the presence of 1 mmol/l ATP or 1 mmol/l ADP, as indicated. Data (means±SEM) are from 3 or 4 experiments in each case, each involving three replicates

for a role for these channels on beta cell mitochondria (Fig. 10). Whether the different intensity profiles of SUR1 and Kir6.2 (showing a greater enrichment of SUR1 on LDCVs; compare Figs. 1, 2 and 5) may be of functional significance is uncertain, but would be consistent with earlier studies [21]. Thus, although we were unable here to demonstrate any role for K_{ATP} channels in intravesicular ion homeostasis, other roles for sulfonylurea binding to vesicles in regulating exocytosis, perhaps mediated by protein kinase C [53], are not excluded.

The subcellular localisation of SUR1, as revealed here using immunocytochemical techniques, is somewhat at variance with the findings of predominant nuclear envelope labelling with glibenclamide-BODIPY-FL in mouse beta cells [22], and might suggest the existence of a population of K_{ATP} channels at this site with a particularly high binding affinity for sulfonylureas. On the other hand, and in contrast to another report using this dye [18], we were able to demonstrate clear immunolabelling of non-dense-core vesicle intracellular membranes with anti-SUR1 antibodies, likely to correspond to ER/Golgi membranes, including the ER-contiguous nuclear envelope. These findings thus support a role for K_{ATP} channels in controlling Ca^{2+} release from the ER into the nucleus, and hence beta cell gene expression [22].

Might dense-core vesicles serve as sorting stations for the trafficking of K_{ATP} channels to the cell surface? This is an intriguing possibility, given that selective deposition of K_{ATP} channels at the plasma membrane during periods of continuous stimulation may contribute to the loss of glucose responsiveness observed in type 2 diabetes.

Acknowledgements Supported by Wellcome Trust Programme Grant 067081/Z/02/Z. We thank M. Jepson and A. Leard (Bristol MRC Imaging Facility) for technical assistance, P. Cullen for the use of the UltraView confocal microscope, and A. Herman for FACS sorting. B. Schwappach and H. Yuan were supported by German Research Foundation Deutsche Forschungsgemeinschaft) Grant SFB638. G. A. Rutter is a Wellcome Trust Research Leave Fellow.

Duality of interest The authors have no conflicts of interest.

References

1. Rutter GA (2001) Nutrient-secretion coupling in the pancreatic islet b-cell: recent advances. Mol Aspects Med 22:247–284
2. Rutter GA (2004) Visualising insulin secretion. Diabetologia 47:1861–1872
3. Aguilar-Bryan L, Bryan J (1999) Molecular biology of adenosine triphosphate-sensitive potassium channels. Endocr Rev 20:101–135
4. Lang JC (1999) Molecular mechanisms and regulation of insulin exocytosis as a paradigm of endocrine secretion. Eur J Biochem 259:3–17
5. Miki T, Liss B, Minami K et al (2001) ATP-sensitive K^+ channels in the hypothalamus are essential for the maintenance of glucose homeostasis. Nat Neurosci 4:507–512
6. Miki T, Nagashima K, Tashiro F et al (1998) Defective insulin secretion and enhanced insulin action in KATP channel-deficient mice. Proc Natl Acad Sci USA 95:10402–10406
7. Seghers V, Nakazaki M, DeMayo F, Aguilar-Bryan L, Bryan J (2000) Sur1 knockout mice—a model for K-ATP channel-independent regulation of insulin secretion. J Biol Chem 275:9270–9277
8. Sharma N, Crane A, Gonzalez G, Bryan J, Aguilar-Bryan L (2000) Familial hyperinsulinism and pancreatic beta-cell ATP-sensitive potassium channels. Kidney Int 57:803–808
9. Dunne MJ, Cosgrove KE, Shepherd RM, Aynsley-Green A, Lindley KJ (2004) Hyperinsulinism in infancy: from basic science to clinical disease. Physiol Rev 84:239–275

10. Sakura H, Wat N, Horton V, Millns H, Turner RC, Ashcroft FM (1996) Sequence variations in the human Kir6.2 gene, a subunit of the beta-cell ATP-sensitive K-channel: no association with NIDDM in white Caucasian subjects or evidence of abnormal function when expressed in vitro. Diabetologia 39:1233–1236
11. Schwanstecher C, Meyer U, Schwanstecher M (2002) KIR6.2 polymorphism predisposes to type 2 diabetes by inducing overactivity of pancreatic beta-cell ATP-sensitive K+ channels. Diabetes 51:875–879
12. Gloyn AL, Weedon MN, Owen KR et al (2003) Large-scale association studies of variants in genes encoding the pancreatic beta-cell K_{ATP} channel subunits Kir6.2 (*KCNJ11*) and SUR1 (*ABCC8*) confirm that the *KCNJ11* E23K variant is associated with type 2 diabetes. Diabetes 52:568–572
13. Gloyn AL, Pearson ER, Antcliff JF et al (2004) Activating mutations in the gene encoding the ATP-sensitive potassium-channel subunit Kir6.2 and permanent neonatal diabetes. N Engl J Med 350:1838–1849
14. Vaxillaire M, Populaire C, Busiah K et al (2004) Kir6.2 mutations are a common cause of permanent neonatal diabetes in a large cohort of French patients. Diabetes 53:2719–2722
15. Massa O, Iafusco D, D'Amato E et al (2004) *KCNJ11* activating mutations in Italian patients with permanent neonatal diabetes. Hum Mutat 25:22–27
16. Suzuki M, Fujikura K, Inagaki N, Seino S, Takata K (1997) Localization of the ATP-sensitive K+ channel subunit Kir6.2 in mouse pancreas. Diabetes 46:1440–1444
17. Suzuki M, Fujikura K, Kotake K, Inagaki N, Seino S, Takata K (1999) Immuno-localization of sulphonylurea receptor 1 in rat pancreas. Diabetologia 42:1204–1211
18. Geng X, Li L, Watkins S, Robbins PD, Drain P (2003) The insulin secretory granule is the major site of K_{ATP} channels of the endocrine pancreas. Diabetes 52:767–776
19. Carpentier JL, Sawano F, Ravazzola M, Malaisse WJ (1986) Internalization of ^{3}H-glibenclamide in pancreatic islet cells. Diabetologia 29:259–261
20. Ozanne SE, Guest PC, Hutton JC, Hales CN (1995) Intracellular localization and molecular heterogeneity of the sulphonylurea receptor in insulin-secreting cells. Diabetologia 38:277–282
21. Barg S, Renstrom E, Berggren PO et al (1999) The stimulatory action of tolbutamide on Ca^{2+}-dependent exocytosis in pancreatic b cells is mediated by a 65-kDa mdr-like P-glycoprotein. Proc Natl Acad Sci USA 96:5539–5544
22. Quesada I, Rovira JM, Martin F, Roche E, Nadal A, Soria B (2002) Nuclear KATP channels trigger nuclear Ca^{2+} transients that modulate nuclear function. Proc Natl Acad Sci USA 99:9544–9549
23. Smith PA, Proks P, Moorhouse A (1999) Direct effects of tolbutamide on mitochondrial function, intracellular Ca^{2+} and exocytosis in pancreatic beta-cells. Pflugers Arch 437:577–588
24. Garlid KD, Paucek P, Yarov-Yarovoy V, Sun X, Schindler PA (1996) The mitochondrial K_{ATP} channel as a receptor for potassium channel openers. J Biol Chem 271:8796–8799
25. Kowaltowski AJ, Seetharaman S, Paucek P, Garlid KD (2001) Bioenergetic consequences of opening the ATP-sensitive K^{+} channel of heart mitochondria. Am J Physiol Heart Circ Physiol 280:H649–H657
26. Busija DW, Katakam P, Rajapakse NC et al (2005) Effects of ATP-sensitive potassium channel activators diazoxide and BMS-191095 on membrane potential and reactive oxygen species production in isolated piglet mitochondria. Brain Res Bull 66:85–90
27. Garlid KD (2000) Opening mitochondrial K_{ATP} in the heart—what happens, and what does not happen. Basic Res Cardiol 95:275–279
28. Ainscow EK, Zhao C, Rutter GA (2000) Acute overexpression of lactate dehydrogenase-A perturbs beta-cell mitochondrial metabolism and insulin secretion. Diabetes 49:1149–1155
29. Yuan H, Michelsen K, Schwappach B (2003) 14-3-3 dimers probe the assembly status of multimeric membrane proteins. Curr Biol 13:638–646
30. Wasmeier C, Hutton JC (1996) Molecular cloning of phogrin, a protein-tyrosine phosphatase homologue localized to insulin secretory granule membranes. J Biol Chem 271:18161–18170
31. Luzio JP, Brake B, Banting G, Howell KE et al (1990) Identification, sequencing and expression of an integral membrane protein of the trans-Golgi network (TGN38). Biochem J 270:97–102
32. Brown MS, Goldstein JL (1997) The SREBP pathway: regulation of cholesterol metabolism by proteolysis of a membrane-bound transcription factor. Cell 89:331–340
33. Ravier MA, Rutter GA (2005) Glucose or insulin, but not zinc ions, inhibit glucagon secretion from mouse pancreatic α-cells. Diabetes 54:1789–1797
34. Molnar E, Varadi A, McIlhinney RAJ, Ashcroft SJH (1995) Identification of functional ionotropic glutamate receptor proteins in pancreatic beta-cells and in islets of Langerhans. FEBS Lett 371:253–257
35. Pouli AE, Emmanouilidou E, Zhao C, Wasmeier C, Hutton JC, Rutter GA (1998) Secretory granule dynamics visualised in vivo with a phogrin-green fluorescent protein chimaera. Biochem J 333:193–199
36. Ihrke G, Martin GV, Shanks MR, Schrader M, Schroer TA, Hubbard AL (1998) Apical plasma membrane proteins and endolyn-78 travel through a subapical compartment in polarized WIF-B hepatocytes. J Cell Biol 141:115–133
37. Erickson PF, Moore BW (1980) Investigation of the axonal transport of three acidic, soluble proteins (14-3-2, 14-3-3, and S-100) in the rabbit visual system. J Neurochem 35:232–241
38. Pouli AE, Kennedy HJ, Schofield JG, Rutter GA (1998) Insulin targeting to the regulated secretory pathway after fusion with green fluorescent protein and firefly luciferase. Biochem J 331:669–675
39. Varadi A, Johnson-Cadwell LI, Cirulli V, Yoon Y, Allan VJ, Rutter GA (2004) Cytoplasmic dynein regulates the subcellular distribution of mitochondria by controlling the recruitment of the fission factor dynamin-related protein-1. J Cell Sci 117:4389–4400
40. Varadi A, Tsuboi T, Rutter GA (2005) Myosin Va transports dense core secretory vesicles in pancreatic MIN6 b-cells. Mol Biol Cell 16:2670–2680
41. Varadi A, Molnar E, Ostenson CG, Ashcroft SJH (1996) Isoforms of endoplasmic reticulum Ca^{2+}-ATPase are differentially expressed in normal and diabetic islets of Langerhans. Biochem J 319:521–527
42. Ainscow EK, Rutter GA (2001) Mitochondrial priming modifies Ca^{2+} oscillations and insulin secretion in pancreatic islets. Biochem J 353:175–180
43. Brini M, Marsault R, Bastianutto C, Alverez J, Pozzan T, Rizzuto R (1995) Transfected aequorin in the measurement of cytosolic Ca^{2+} concentration ([Ca^{2+}]). A critical evalulation. J Biol Chem 270:9896–9903
44. Mitchell K, Pinton P, Varadi A et al (2001) Dense core secretory vesicles revealed as a dynamic Ca^{2+} store in neuroendocrine cells with a VAMP2.aequorin chimaera. J Cell Biol 155:41–51
45. Mitchell KJ, Tsuboi T, Rutter GA (2004) Role for plasma membrane-related Ca^{2+}-ATPase-1 (PMR1 / ATP2C1) in pancreatic b-cell Ca^{2+} homeostasis revealed by RNA silencing. Diabetes 53:393–400
46. Cobbold PH, Rink TJ (1987) Fluorescence and bioluminescence measurement of cytoplasmic free calcium. Biochem J 248:313–328
47. Rutter GA, Denton RM (1988) Regulation of NAD^{+}-linked isocitrate dehydrogenase and 2-oxoglutarate dehydrogenase by Ca2+ ions within toluene-permeabilized rat heart mitochondria. Interactions with regulation by adenine nucleotides and NADH/NAD+ ratios. Biochem J 252:181–189 (published erratum appears in Biochem J 1988; 253:935)
48. Rutter GA, Theler J-M, Murta M, Wollheim CB, Pozzan T, Rizzuto R (1993) Stimulated Ca^{2+} influx raises mitochondrial free Ca^{2+} to supramicromolar levels in a pancreatic b-cell line: possible role in glucose and agonist-induced insulin secretion. J Biol Chem 268:22385–22390

49. Rizzuto R, Simpson AWM, Brini M, Pozzan T (1992) Rapid changes of mitochondrial Ca^{2+} revealed by specifically targeted recombinant aequorin. Nature 358:325–327
50. Grimmsmann T, Rustenbeck I (1998) Direct effects of diazoxide on mitochondria in pancreatic B-cells and on isolated liver mitochondria. Br J Pharmacol 123:781–788
51. Halestrap AP, Brenner C (2003) The adenine nucleotide translocase: a central component of the mitochondrial permeability transition pore and key player in cell death. Curr Med Chem 10:1507–1525
52. Kennedy HJ, Pouli AE, Jouaville LS, Rizzuto R, Rutter GA (1999) Glucose-induced ATP microdomains in single islet beta-cells. J Biol Chem 274:13281–13291
53. Eliasson L, Renstrom E, Ammala C et al (1996) PKC-dependent stimulation of exocytosis by sulfonylureas in pancreatic beta cells. Science 271:813–815